Journal of Integrative Neuroscience

J. Integr. Neurosci. **2026**; 25(11): 50938
https://doi.org/10.31083/JIN50938

Original Research

Aurantio-Obtusin Suppresses Glioblastoma Growth by Inducing Oxidative Stress

Jin Liao[1,2,†], Junrong Zhang[2,†], Xinyi Zheng[3], Ailin Qu[3], Lingling Li[3], Jianghan Zhao[3], Zhengjun Zhou[4,5,*], Hengzhu Zhang[1,6,*]

[1]Department of Neurosurgery, Northern Jiangsu People's Hospital Affiliated to Yangzhou University, 225001 Yangzhou, Jiangsu, China
[2]Department of Neurosurgery, Suining First People's Hospital, 629019 Suining, Sichuan, China
[3]School of Clinical Medicine, Southwest Medical University, 646000 Luzhou, Sichuan, China
[4]Department of Neurosurgery, The Affiliated Hospital, Southwest Medical University, 646000 Luzhou, Sichuan, China
[5]Sichuan Clinical Research Center for Neurosurgery, The Affiliated Hospital, Southwest Medical University, 646000 Luzhou, Sichuan, China
[6]Department of Neurosurgery, Northern Jiangsu People's Hospital, 225001 Yangzhou, Jiangsu, China
*Correspondence: zzj000026@yeah.net (Zhengjun Zhou); zhanghengzhu@sina.com (Hengzhu Zhang)
[†]These authors contributed equally.
Academic Editor: Bettina Platt
Submitted: 11 February 2026 Revised: 17 June 2026 Accepted: 3 July 2026 Published: 3 November 2026

Abstract

Objectives: Aurantio-obtusin (AO), a bioactive compound and an analogue of the anticancer drug doxorubicin (DOX), possesses anticancer, anti-inflammatory, and antioxidant properties. However, the effect of AO on glioblastoma (GB) remains unclear. **Methods:** The viability of AO-treated GB cells was evaluated using the Cell Counting Kit-8 (CCK-8) and 5-Ethynyl-2′-deoxyuridine (EdU) staining assays. Flow cytometry was used to analyze the effects of AO treatment on the cell cycle and apoptosis of GB cells. Levels of reactive oxygen species (ROS), malondialdehyde (MDA), and glutathione (GSH) in AO-treated GB cells were measured to assess cellular oxidative stress. For the *in vivo* experiments, four-week-old female BALB/c nude mice were used. **Results:** AO dose-dependently inhibited GB cell viability and promoted apoptosis. Treatment with AO led to increased ROS production in GB cells, which in turn induced DNA damage and G2/M phase arrest. Concurrently, the phosphorylation level of cdc2 and the expression of cleaved-caspase-3 and gamma-H2AX (γ-H2AX) were significantly increased in AO-treated GB cells. Notably, the effects of AO on the GB cell cycle and apoptosis were attenuated by the ROS scavenger acetylcysteine (AC). Furthermore, AO treatment significantly inhibited tumor growth *in vivo*. **Conclusion:** The results suggest that AO may inhibit GB cell growth by inducing oxidative stress, indicating that AO is a promising agent for the treatment of GB.

Keywords: glioblastoma; aurantio-obtusin; reactive oxygen species; cell cycle; apoptosis

1. Introduction

Glioblastoma (GB) is the most common primary malignant brain tumor in adults, characterized by rapid progression, high invasiveness, and uniformly poor prognosis [1,2]. Current therapies, including surgical resection, radiotherapy, and chemotherapy, remain inadequate for effectively treating GB [3,4,5]. Severe adverse effects and drug resistance continue to pose significant challenges in clinical practice [6,7]. Consequently, developing novel therapeutic agents has become highly significant for the improvement of clinical outcomes for GB patients.

Historically, traditional Chinese medicine and its extracted components have played a significant role in cancer treatment due to their favorable therapeutic effects and low cost [8]. To enhance the effectiveness of existing anticancer regimens, the anticancer properties of natural bioactive compounds have received widespread attention in complementary approaches for various cancers. For example, compounds derived from plants and fungi have been identified as ideal candidates for combination therapy or adjuvant therapy in the treatment of GB [9,10]. Aurantio-obtusin (AO) is a key active component extracted from the seeds of the traditional Chinese herb Cassia, which have long been used for clearing heat, improving vision, and relieving constipation [11]. Initially, research on AO focused on its anti-inflammatory and hepatoprotective activities [12,13,14]. More recently, with in-depth exploration of the antitumor potential of natural products, AO has attracted widespread interest in oncology research due to its significant inhibitory effects on breast and liver cancer [15,16]. This study aims to evaluate whether AO exhibits therapeutic efficacy against GB and to define the functional basis of this effect.

Reactive oxygen species (ROS) are a class of highly reactive chemical species, including superoxide anions, hydrogen peroxide, and hydroxyl radicals [17,18]. In tumors, due to upregulated metabolic rates, endogenous ROS levels in cancer cells are often elevated [19]. Moderately increased ROS acts as a second messenger, activating multiple pro-tumor signaling pathways and inducing genomic in-

Copyright: © 2026 The Author(s). Published by IMR Press.
This is an open access article under the CC BY 4.0 license.

Publisher's Note: IMR Press stays neutral with regard to jurisdictional claims in published maps and institutional affiliations.

stability, thereby promoting tumor progression [20]. However, when ROS levels exceed the antioxidant buffering capacity of cells, they can lead to severe DNA damage, cell cycle imbalance, and even apoptosis [21,22]. Previous studies have suggested that inducing oxidative stress to generate excessive ROS in cancer cells may represent a novel and selective anticancer strategy [23,24]. In this study, it was first confirmed that AO could induce cell apoptosis by triggering massive ROS production, thereby inhibiting the malignant progression of GB. In conclusion, these findings indicate that AO is a potential therapeutic agent for GB.

2. Materials and Methods

2.1 Chemicals and Reagents

AO (HY-N0261, purity: 99.89%) and acetylcysteine (AC, HY-B0215, purity: 99.86%) were purchased from MedChemExpress (Monmouth Junction, NJ, USA). Stock solutions of AO and AC were prepared in DMSO (D2650, Sigma-Aldrich, Louis, MO, USA) at 200 mM and kept at –20 °C until use. The final DMSO concentration in all cell culture experiments was maintained below 0.1%.

2.2 Cell Culture

The human astrocyte (HA; 1800, ScienCell, Carlsbad, CA, USA), U87 (HTB-14, ATCC, Manassas, VA, USA; RRID: CVCL_0022; note: this line differs from the original Uppsala University U-87MG line), and U251 (09063001, ECACC, Salisbury, UK) were propagated in DMEM (SH30243, HyClone, Logan, UT, USA) with 10% FBS (10099141, Thermo Fisher Scientific, Waltham, MA, USA) and 1% penicillin-streptomycin (15140122, Thermo Fisher Scientific), at 37 °C in a humidified 5% CO_2 incubator (51023126, Thermo Fisher Scientific). Before AO treatment, cells were allowed to stabilize for more than 24 h. For all experiments, HA, U87, and U251 were used at passages 2 and 4. All cells used in this study were authenticated by short tandem repeat (STR) analysis and confirmed to be free of mycoplasma contamination by PCR-based detection.

2.3 Cell Viability

Cells (1×10^3/well) were seeded in 96-well plates (3599, Corning, Shanghai, China), allowed to attach overnight, and then exposed to treatments for 24 or 48 h, after which viability was assessed with the cell counting kit-8 (CCK-8; CK04, Dojindo, Kumamoto, Japan). Cell proliferation was also assessed by manual counting under a microscope (DM2000 LED, Leica, Wetzlar, Germany). All experiments were performed with a minimum of three replicates.

2.4 5-Ethynyl-2′-Deoxyuridine (EdU) Assay

GB cells were seeded into 35 mm confocal dishes (3294, Corning) and cultured overnight. After attachment, cells were treated with various concentrations of AO (0, 20, 40, 80 μM) for 24 h. For EdU labeling, 10 μM EdU (BeyoClicTM EdU Cell Proliferation Kit with AF647, C0081S, Beyotime, Shanghai, China) was added to the culture medium during the last two hours of the treatment period. Following EdU labeling, cells underwent fixation (4% PFA (BL539A, Biosharp, Anhui, China), 20 min, room temperature (RT)) and subsequent permeabilization (0.3% Triton X-100 (T8787, MilliporeSigma, Burlington, MA, USA), 10 min). Nuclei were counterstained with 4′,6-diamidino-2-phenylindole (DAPI; C0065, Solarbio, Beijing, China). Stained cells were observed under a fluorescence microscope (Eclipse E400, Nikon, Tokyo, Japan), and three random fields of view with comparable cellular confluence were selected per dish for imaging. The percentage of EdU-positive nuclei among DAPI-stained cells was calculated with ImageJ 1.51 (National Institutes of Health, Bethesda, MD, USA) to determine the proliferation rate.

2.5 Flow Cytometry

For cell cycle analysis, GB cells were stained with propidium iodide (PI) using a cell cycle staining kit (C1008S, Beyotime, China) according to the manufacturer's instructions. The gating strategy was as follows: first, cell debris was excluded on a forward scatter area (FSC-A) versus side scatter area (SSC-A) plot; second, doublets were removed on an FSC-A versus FSC-height (FSC-H) plot; third, single cells were analyzed for PI fluorescence on a linear scale, and cell cycle distribution (G0/G1, S, and G2/M phases) was determined using the Watson model in FlowJo. For apoptosis analysis, cells were stained with an Annexin V-fluorescein isothiocyanate (FITC) apoptosis detection kit (C1062M, Beyotime, China). The gating strategy was as follows: debris was first excluded on FSC-A versus SSC-A; doublets were then excluded on FSC-A versus FSC-H; finally, single cells were displayed on an Annexin V-FITC versus PI quadrant plot. For intracellular ROS measurement, cells were incubated with 2′,7′-dichlorodihydrofluorescein diacetate (DCFH-DA; S1105S, Beyotime, China). The gating strategy was as follows: debris was excluded on FSC-A versus SSC-A; doublets were excluded on FSC-A versus FSC-H; and DCF fluorescence was then analyzed on a FITC channel histogram. Briefly, GB cells were seeded in six-well plates (5×10^4 cells/well) and incubated for 24 h. After treatment of the cells, flow cytometry (CytoFLEX LX, Beckman Coulter, CA, USA) operations were performed on the cells in accordance with the manufacturer's instructions.

2.6 Detection of Malondialdehyde (MDA) and Glutathione (GSH)

The concentrations of MDA and GSH were quantified with respective commercial detection kits (S0131 and S0053, Beyotime), following the protocols provided by the manufacturer. Specifically, MDA levels were assessed based on absorbance at 532 nm, and GSH levels were evaluated by absorbance at 405 nm. Finally, the obtained

raw data were respectively normalized to the corresponding mean values of the control group in each assay, and the results were expressed as relative levels.

2.7 Immunofluorescence

U87 cells (1×10^5 cells/well) were seeded into 24-well plates and cultured overnight before exposure to AO. Following treatment, cells underwent sequential fixation (4% PFA, 30 min), permeabilization (1% Triton X-100, 15 min), and blocking (1% bovine serum albumin (BSA; A8020, Solarbio)). Primary antibody (rabbit anti-γ-H2AX, ab81299, 1:200; Abcam, Cambridge, UK) was applied overnight at 4 °C, after which the cells were rinsed thrice with PBS and incubated for 1 h at RT with secondary antibody (Alexa Fluor™ 488-conjugated goat anti-rabbit IgG, ab150077, 1:1000; Abcam). Mounting was performed with ProLong™ Diamond Antifade containing DAPI (C0065, Solarbio). All images were captured with a fluorescence microscope and analyzed quantitatively using ImageJ software 1.51.

2.8 Western Blot

U87 cells and tumor tissues were collected and lysed using radioimmunoprecipitation assay (RIPA) buffer (P0013B, Beyotime) supplemented with phosphatase and protease inhibitors. Total protein concentration was measured via the BCA assay. Protein extracts were then separated on 10% sodium dodecyl sulfate-polyacrylamide gel electrophoresis (SDS-PAGE) gels and electrotransferred onto polyvinylidene fluoride membranes (ISEQ00010, MilliporeSigma). Following transfer, membranes were blocked with a protein-free rapid blocking solution (PS108P, EpiZyme, Shanghai, China). Primary antibody incubation was performed overnight at 4 °C using the following: Rabbit anti-phospho-cell division cycle 2 (cdc2) (9111, 1:1000; Cell Signaling Technology, Danvers, MA, USA), rabbit anti-cdc2 (77055, 1:1000; Cell Signaling Technology), rabbit anti-B-cell lymphoma 2 (Bcl-2) (12789-1-AP, 1:1000; Proteintech, Wuhan, China;), cleaved caspase-3 (25128-1-AP, 1:1000; Proteintech), rabbit anti-γ-H2AX (ab81299, 1:2000; Abcam), and mouse anti-GAPDH (AG019, 1:2000; Beyotime). Subsequently, the membranes were probed with appropriate secondary antibodies for one hour at room temperature. Signal detection was carried out using a sensitive chemiluminescence test kit (SQ201, EpiZyme), and band intensities were quantified with ImageJ software 1.51.

2.9 GB Xenograft Model

The subcutaneous xenograft tumor model is a common approach for evaluating the direct antitumor effects of drugs and elucidating their underlying molecular mechanisms [25]. BALB/c nude mice are an inbred, immunodeficient strain characterized by congenital athymia and consequent T-cell deficiency, which allows successful engraftment of human tumor cells without immune rejection. Ten healthy four-week-old female BALB/c nude mice (16–18 g) were acquired from GemPharmatech Co., Ltd. (Chengdu, China). They were housed in a specific pathogen-free (SPF)-grade animal facility under controlled conditions: Indoor temperature of 22 ± 2 °C with a 12/12-hour light/-dark cycle, with adequate food and water. The mice were acclimatised to the housing facility for seven days before the start of the experiment. The U87 cell suspension (1×10^5 cells) was subcutaneously injected into one side of the mouse axilla using a sterile syringe. Subsequently, the tumor-bearing mice were randomly divided into two groups (the control and AO treatment groups, n = 5/group). The investigators who administered treatments and assessed outcomes (including tumor volume, bioluminescence imaging, H&E staining, and immunofluorescence) were blinded to group allocation. *In vitro* samples were coded and analyzed by blinded investigators. Beginning on the second day after cell implantation, the mice were intraperitoneally administered either normal saline or AO (20 mg/kg) once daily for three consecutive weeks, and their body weight was recorded daily. At the end of the experiment, mice were deeply anesthetized with sodium pentobarbital (50 mg/kg, i.p.), euthanized by cervical dislocation, and then tumor specimens were collected for volume measurement.

2.10 Immunohistochemical Staining

Paraffin-embedded mouse tumor tissue was sectioned and underwent deparaffinization in xylene (108298, MilliporeSigma), rehydration in a graded ethanol series, and a final rinse with double-distilled water. Antigen retrieval was accomplished via microwave heating in citrate buffer (C9999, MilliporeSigma), after which endogenous peroxidases were quenched with hydrogen peroxide and nonspecific binding was minimized by bovine serum albumin treatment. Primary antibody incubation (rabbit anti-ki67, ab15580, dilution 1:200; Abcam) was carried out overnight. After PBS washing, sections were exposed to biotin-labeled goat anti-rabbit IgG (A0277, 1:100; Beyotime) for one hour. Visualization used the chromogen 3,3′-diaminobenzidine (D4418, MilliporeSigma). Following hematoxylin (C0105S, Beyotime) counterstaining, sections were dehydrated and mounted with neutral resin (G8590, Solarbio). Finally, stained slides were observed and photographed under a microscope (DM2000 LED, Leica, Wetzlar, Germany).

2.11 Statistical Analysis

Statistical analyses were performed on GraphPad Prism 8.0 (GraphPad Software, San Diego, CA, USA), with data expressed as means ± standard error of the mean (SEM). Normality and variance homogeneity were confirmed by Shapiro-Wilk and Levene's tests, respectively; all variables met these assumptions, so parametric tests were adopted. Two-group comparisons employed the *t*-test,

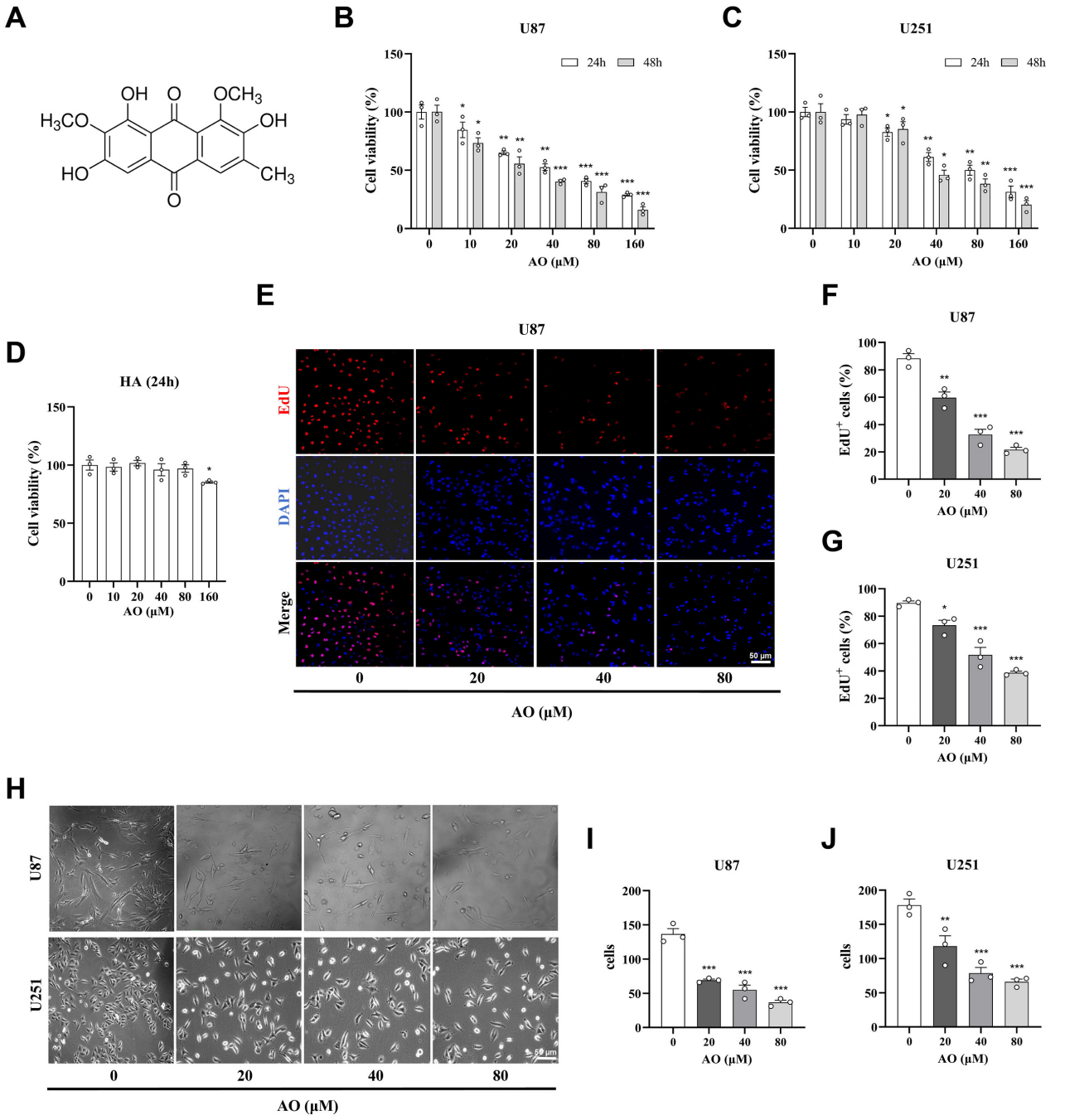


Fig. 1. AO treatment inhibits GB cell proliferation. (A) The chemical structure of AO. (B,C) CCK-8 measured cell viability after treatment of U87 and U251 cells with different concentrations of AO for 24 and 48 h. (D) The cell viability of HA cells after being treated with different concentrations of AO for 24 hours was measured by CCK-8. (E) Representative images of EdU staining of U87 cells. Scale bar: 50 μm. (F,G) EdU staining statistical results of U87 and U251 cells. (H) Microscopic representative images of U87 and U251 cells. Scale bar: 50 μm. (I,J) The statistical results of cell numbers for U87 and U251. n = 3/group, $^{*}p < 0.05$, $^{**}p < 0.01$ and $^{***}p < 0.001$ vs. "0" control group. AO, aurantio-obtusin; GB, glioblastoma; CCK-8, cell counting kit-8; HA, human astrocyte; EdU, 5-Ethynyl-2′-deoxyuridine.

whereas comparisons involving three or more groups utilized one-way analysis of variance (ANOVA). Statistical significance was defined as $p < 0.05$.

3. Results

3.1 AO Treatment Inhibits GB Cell Proliferation

The chemical structure of AO is given in Fig. 1A. First, the anti-proliferative activity of AO against GB was investigated *in vitro* using two GB cell lines (U87 and

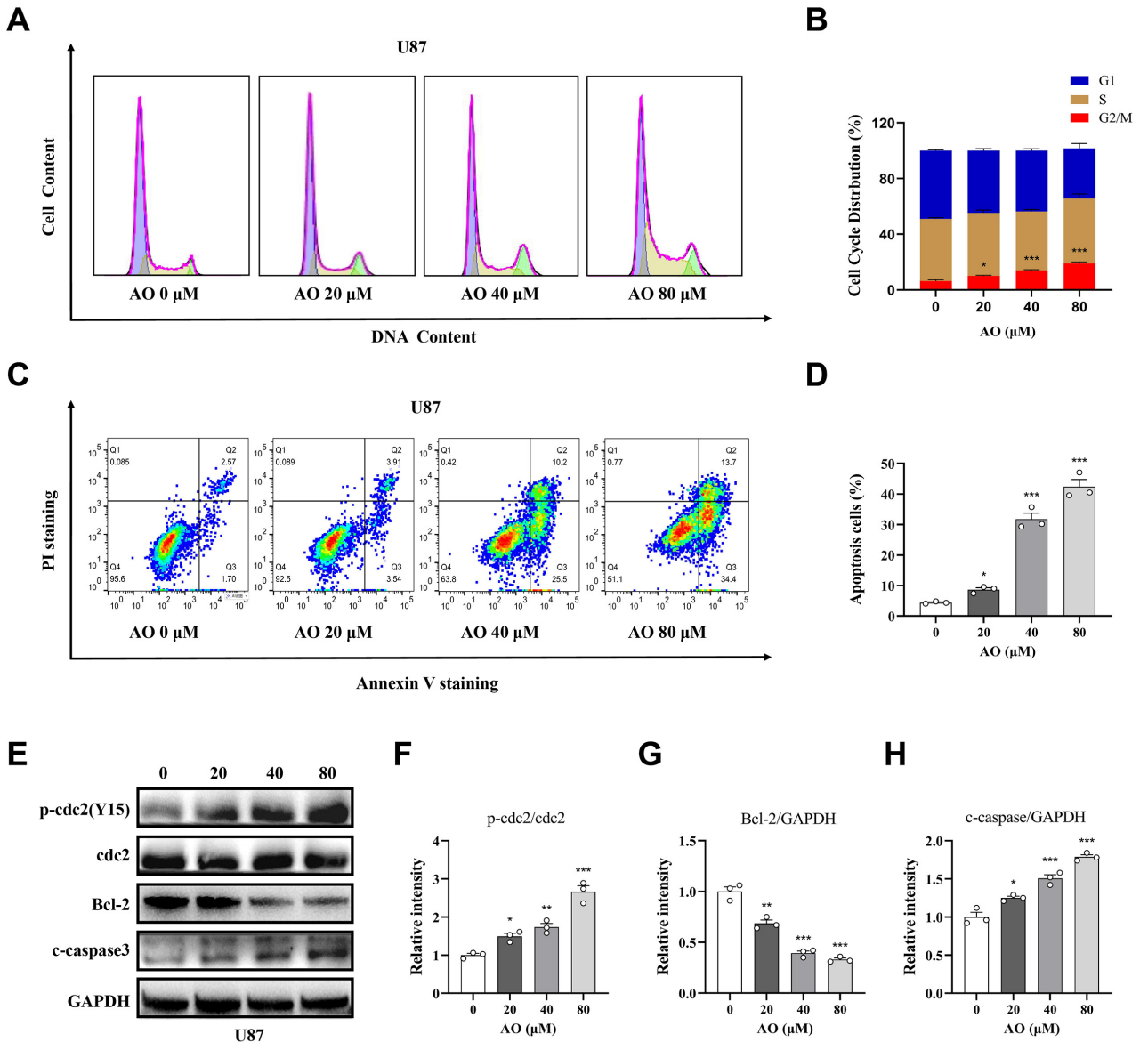


Fig. 2. AO treatment induces G2/M phase arrest and apoptosis in GB. (A,B) Representative results and statistical analysis of the cell cycle distribution in U87 cells analyzed by flow cytometry. (C,D) Representative results and statistical analysis of apoptosis in U87 cells analyzed by flow cytometry. (E–H) Western blot analysis of the levels of p-cdc2, cdc2, Bcl-2, and cleaved caspase-3 in U87 cells. n = 3/group, $^{*}p < 0.05$, $^{**}p < 0.01$, and $^{***}p < 0.001$ vs. "0" control group. PI, propidium iodide; cdc2, cell division cycle 2; Bcl-2, B-cell lymphoma 2; GAPDH, glyceraldehyde-3-phosphate dehydrogenase.

U251). Both cell lines were incubated with varying concentrations of AO (0–160 μM) for 24 or 48 hours, after which cell proliferation was assessed. The CCK-8 assay results showed that AO inhibited the proliferative activity of U87 and U251 cells in a concentration- and time-dependent manner (Fig. 1B,C). Subsequently, it was also found that AO at concentrations below 160 μM had no significant effect on the viability of HA cells (Fig. 1D), indicating its selective killing effect on GB cells. After 24 hours of treatment with 40 μM AO, the inhibition rate of GB cell viability reached approximately 50%. Therefore, subsequent experiments were conducted using AO at concentrations of 20, 40, and 80 μM for 24 hours. EdU staining results demonstrated that AO treatment significantly reduced the proportion of EdU-positive GB cells (Fig. 1E–G). To further visually confirm the inhibitory effect of AO on GB cell proliferation, a microscope was employed for cell counting. Results revealed a marked decrease in the proliferative activity of AO-treated GB cells, as evidenced by a significantly lower cell count in the AO treatment groups when compared to the control group (Fig. 1H–J). These data collectively point to a potent antiproliferative effect of AO on GB cells.

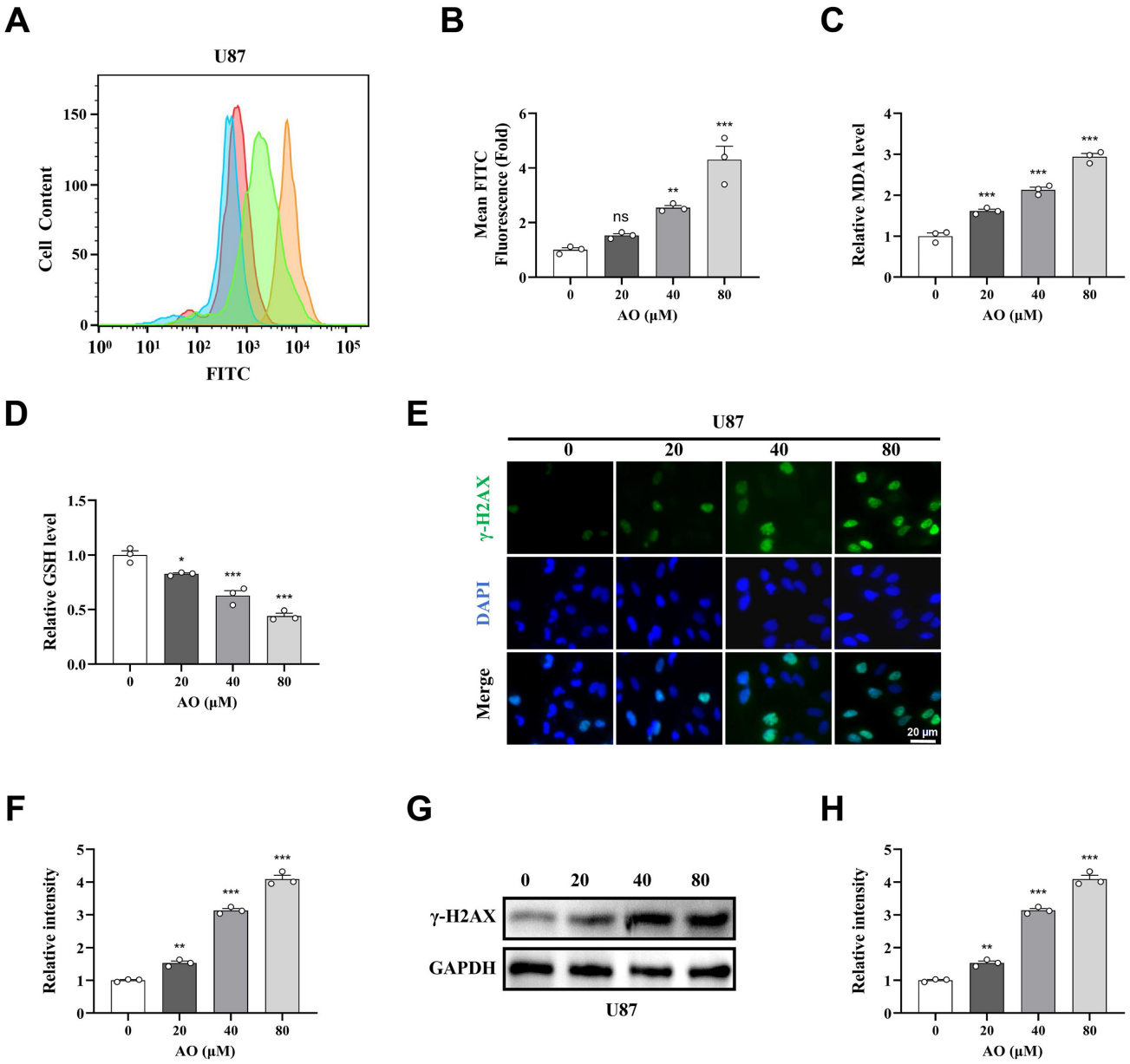


Fig. 3. AO treatment induces the generation of ROS and leads to DNA damage in GB. (A,B) Representative results and statistical analysis of ROS levels in U87 cells. (C) Statistical analysis of MDA levels in U87 cells. (D) Statistical analysis of GSH levels in U87 cells. (E,F) Representative immunofluorescence images and quantitative analysis of γ-H2AX in U87 cells. Scale bar: 20 μm. (G,H) Western blot analysis of the levels of γ-H2AX in U87 cells. n = 3/group, "ns" indicates no statistical difference, $^{*}p < 0.05$, $^{**}p < 0.01$, and $^{***}p < 0.001$ vs. "0" control group. FITC, fluorescein isothiocyanate; DAPI, 4′,6-diamidino-2-phenylindole; ROS, reactive oxygen species; MDA, malondialdehyde; GSH, glutathione; γ-H2AX, gamma-H2AX.

3.2 AO Treatment Induces G2/M Phase Arrest and Apoptosis in GB

To further explore the potential mechanisms underlying the anti-GB activity of AO, the cell cycle distribution and apoptosis in AO-treated U87 cells were analyzed. Flow cytometry analysis showed that AO increased the proportion of U87 cells in the G2/M phase in a concentration-dependent manner (Fig. 2A,B). Simultaneously, AO significantly promoted apoptosis in U87 cells (Fig. 2C). Specifically, compared with the control group (approximately 5%), the proportion of apoptotic U87 cells increased to approximately 10% under 20 μM AO, to 30% under 40 μM, and exceeded 40% under 80 μM (Fig. 2D). Cdc2 is a known key regulator of the transition from G2 to M phase [26]. Previous studies have confirmed that phosphorylation at tyrosine 15 inhibits cdc2 activity and is one of the most important mechanisms leading to G2/M phase arrest [27,28]. To determine whether the G2 phase arrest induced by AO in U87 cells is mechanistically linked to cdc2 phosphorylation, we examined the tyrosine 15 (Tyr15) phosphorylation status by

Western blot and found a concentration-dependent increase (Fig. 2E,F). Additionally, we evaluated the effects of AO on Bcl-2 and cleaved caspase-3 in U87 cells (Fig. 2G,H). Results indicated that AO treatment led to a concentration-dependent decrease in Bcl-2 protein levels and increased cleaved caspase-3 protein levels. These findings indicate that AO induces G2/M phase arrest and apoptosis in GB cells.

3.3 AO Treatment Induces the Generation of ROS and Leads to DNA Damage in GB

ROS exhibits a dose-dependent "double-edged sword" relationship with tumor cell cycle progression and apoptosis. Excessively high ROS levels trigger the DNA damage response and checkpoint activation, resulting in cell cycle arrest [29]. Meanwhile, elevated ROS levels induce mitochondrial membrane permeability transition and modulate the balance of Bcl-2 family proteins, thereby activating the caspase cascade and ultimately initiating the apoptotic program [30]. Previous studies have demonstrated that the antitumor activity of many anthracycline chemotherapeutic agents relies on increasing intracellular ROS levels in tumor cells, leading to DNA damage, cell cycle arrest, and apoptosis [31,32]. As AO is an analog of the anthracycline drug doxorubicin (DOX), it was hypothesized that the efficacy of AO against GB may be associated with its regulation of intracellular ROS levels in GB cells.

To further validate this hypothesis, ROS levels in AO-treated U87 cells were assessed. Flow cytometry results revealed that AO increased ROS generation in U87 cells in a dose-dependent manner (Fig. 3A,B). Furthermore, it was found that AO treatment elevated malondialdehyde (MDA) while decreasing glutathione (GSH) levels in U87 cells (Fig. 3C,D). Immunofluorescence and Western blot analyses demonstrated a significant increase in gamma-H2AX (γ-H2AX), a common biomarker of DNA damage, in AO-treated U87 cells (Fig. 3E–H). Collectively, these results indicate that AO induces high levels of ROS and DNA damage in GB cells.

3.4 Antioxidant AC Abolishes the Anti-GB Effects of AO

To clarify whether ROS generation serves as a key mechanism underlying AO-induced suppression of GB proliferation, G2/M phase arrest, and apoptosis, the antioxidant AC, a potent scavenger of intracellular ROS, was employed. First, it was confirmed that AC (100 μM) effectively reversed the elevation of ROS levels in U87 cells treated with AO (80 μM) (Fig. 4A,B). Subsequently, CCK-8 assays demonstrated that AC significantly rescued the decrease in U87 cell viability caused by AO treatment (Fig. 4C). Furthermore, AC markedly reduced the proportion of U87 cells in the G2/M phase and decreased apoptosis levels following AO exposure (Fig. 4D–G). Consistent with these findings, Western blot analysis revealed that AC substantially counteracted the effects of AO on the phosphorylation level of cdc2, as well as the expression of γ-H2AX and cleaved caspase-3 (Fig. 4H–K). These results indicate that induction of ROS generation may be a critical factor in the anti-GB activity of AO.

3.5 AO Inhibits the Growth of Glioma Xenografts in Mice

Next, a subcutaneous glioma model was generated in mice by injecting U87 cells, and AO was then administered intraperitoneally for three weeks. Results showed that continuous intraperitoneal administration of AO for three weeks significantly reduced tumor volume in GB-bearing mice when compared to the control group (Fig. 5A,B). Notably, body weight did not differ between the two groups, and all AO-treated mice survived, suggesting that AO was well tolerated (Fig. 5C). Immunohistochemical analysis revealed a marked reduction in Ki67 levels in tumor tissues from the AO-treated group (Fig. 5D,E). Additionally, the level of MDA in the tumor tissue of the AO-treated group was significantly increased, while the content of GSH was significantly decreased (Fig. 5F,G). AO treatment significantly elevated the phosphorylation of cdc2 and the protein expression of γ-H2AX and cleaved caspase-3 in tumor tissues relative to controls (Fig. 5H,I). These observations collectively indicate that AO exerts effective anti-GB activity *in vivo*.

4. Discussion

Despite aggressive multimodal treatment, GB remains one of the most lethal malignancies, with a dismal prognosis largely due to inherent or acquired therapeutic resistance [33]. Therefore, developing novel therapeutic agents with distinct mechanisms of action is needed. In this study, a novel anthraquinone derivative, AO, was identified as a potent anti-GB agent. It was demonstrated for the first time that AO exerts its anti-tumor effects by inducing excessive ROS generation, leading to cell cycle arrest at the G2/M phase, apoptosis, and DNA damage in both types of GB cells (Fig. 6).

Initial findings confirmed the robust anti-proliferative effect of AO on GB cell lines (U87 and U251), which was both concentration- and time-dependent. This was further corroborated by EdU incorporation assays and direct cell counting, supporting the conclusion that AO directly inhibits GB cell proliferation. Mechanistically, it was found that AO treatment triggered a significant G2/M phase arrest and induced apoptosis in U87 cells. The G2/M checkpoint is a critical guardian against genomic instability, and its activation often serves as a cellular response to DNA damage [34]. The observation that AO treatment upregulated the phosphorylation of cdc2 at Tyr15, a key inhibitory modification that halts the G2/M transition, provides a molecular link to the observed cell cycle blockade. Concurrently, the shift in the balance of apoptosis-regulating proteins, characterized by downregulation of Bcl-2 and upregulation of

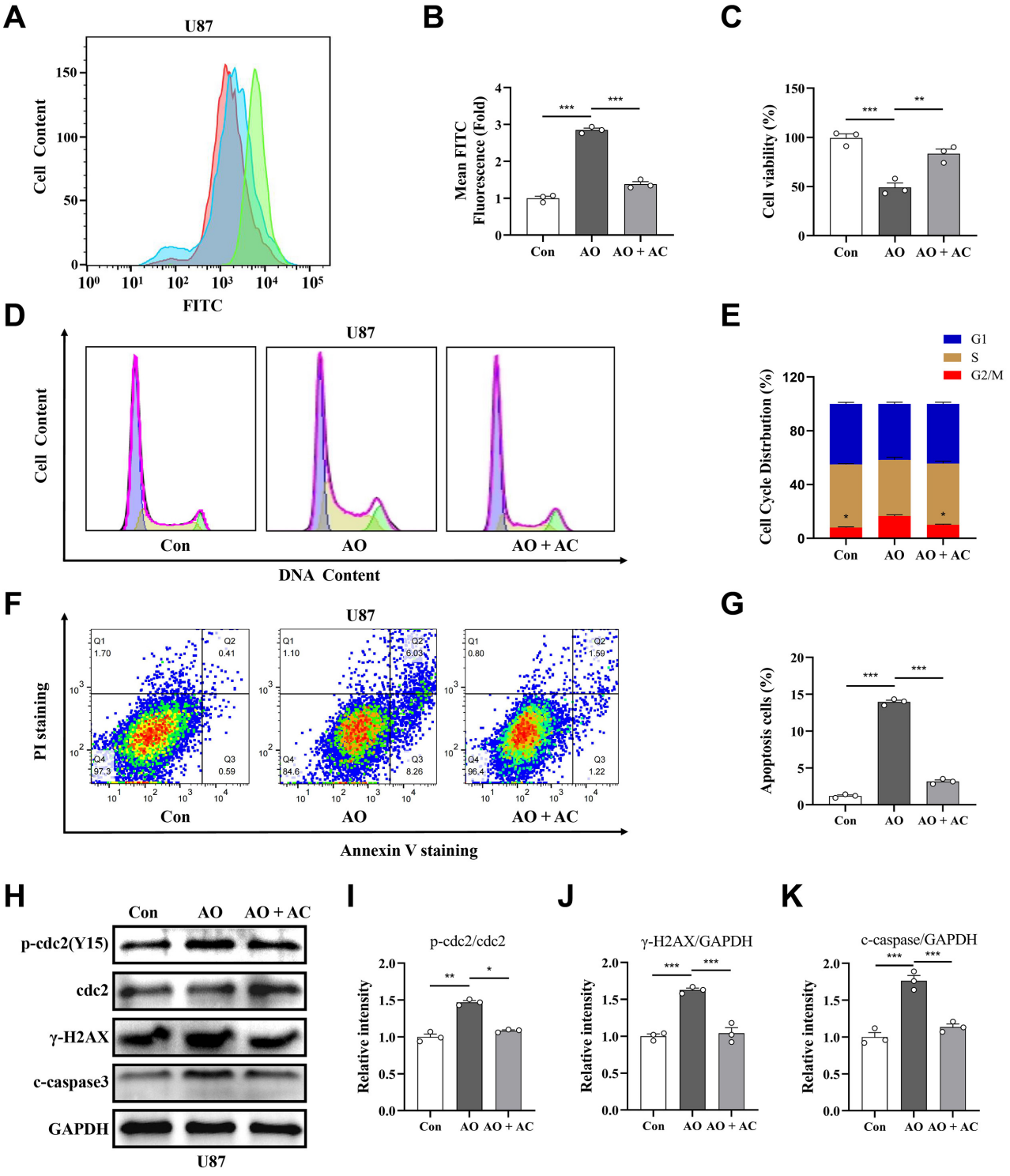


Fig. 4. Antioxidant AC abolishes the anti-GB effects of AO. (A,B) ROS production in U87 cells was analyzed by flow cytometry. (C) The cell viability of U87 was determined by CCK-8. (D,E) Cell cycle phase distribution analyzed by flow cytometry, showing representative profiles and quantitative comparisons. (F,G) Apoptotic rates of U87 cells were evaluated via flow cytometry. (H–K) Western blot analysis of the levels of p-cdc2, cdc2, γ-H2AX, and cleaved caspase-3 in U87 cells. n = 3/group, $^{*}p < 0.05$, $^{**}p < 0.01$, and $^{***}p < 0.001$ vs. "AO" group. Cells were treated with the indicated concentrations of AO (80 μM) alone or in combination with AC (100 μM) for 24 hours. AC, acetylcysteine.

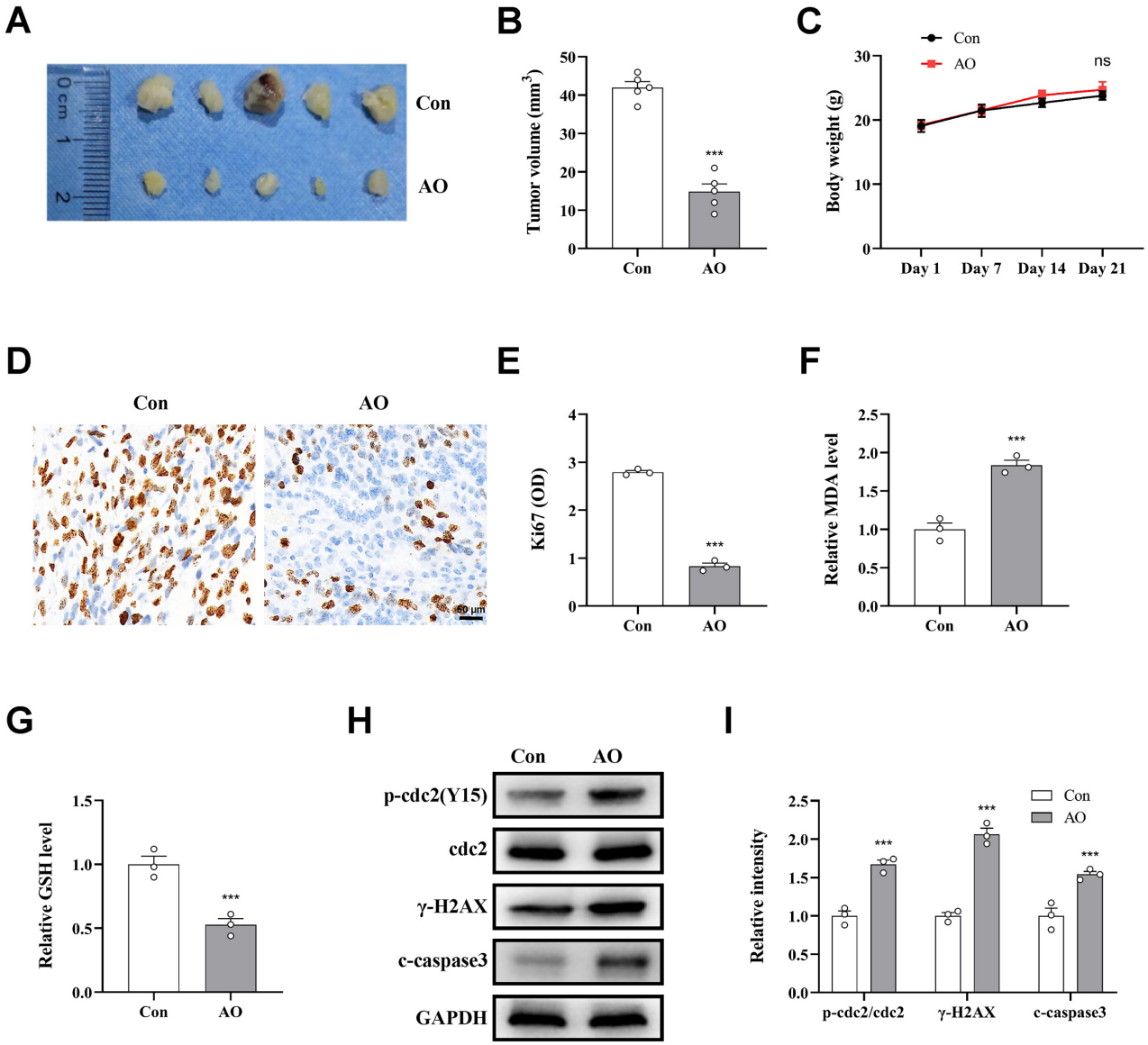


Fig. 5. AO inhibits the growth of glioma xenografts in mice. (A,B) Representative images of tumors and statistical analysis of tumor volume. n = 5/group, $^{***}p < 0.001$ vs. "Con" group. (C) Statistical analysis of mouse body weight. n = 5/group, "ns" indicates no statistical difference. (D,E) Immunohistochemical quantification of tumor proliferation based on Ki67 staining. Scale bar: 50 μm. n = 3/group, $^{***}p < 0.001$ vs. "Con" group. (F) Statistical analysis of MDA levels in tumor tissues. n = 3/group, $^{***}p < 0.001$ vs. "Con" group. (G) Statistical analysis of GSH levels in tumor tissues. n = 3/group, $^{***}p < 0.001$ vs. "Con" group. (H,I) Western blot analysis of the levels of p-cdc2, cdc2, γ-H2AX, and cleaved caspase-3 in tumor tissues. n = 3/group, $^{***}p < 0.001$ vs. "Con" group.

cleaved caspase-3, strongly indicates activation of the mitochondrial apoptotic pathway.

AO has been reported to possess remarkable therapeutic value. One study demonstrated that AO induces nitric oxide (NO) production and promotes vasodilation by regulating the phosphoinositide 3-kinase (PI3K)/protein kinase B (Akt)/endothelial nitric oxide synthase (eNOS) signaling pathway [35]. Additionally, AO exerts anti-inflammatory effects through inhibition of the NF-κB signaling pathway [12]. Liu et al. [16] found that AO suppresses the Akt/mechanistic target of rapamycin (mTOR) signaling pathway, thereby increasing the sensitivity of hepatocellular carcinoma cells to ferroptosis. The most pivotal finding of this study centers on the role of ROS. Anthracyclines like DOX are known to exert part of their cytotoxicity through ROS-mediated mechanisms [36]. As a structural analog of DOX, it was hypothesized that AO may share this property. Indeed, the data clearly show that AO induces a dose-dependent surge in intracellular ROS levels, accompanied by increased lipid peroxidation (elevated MDA) and depletion of the key antioxidant GSH. This pro-oxidant state culminated in significant DNA damage, as evidenced by the

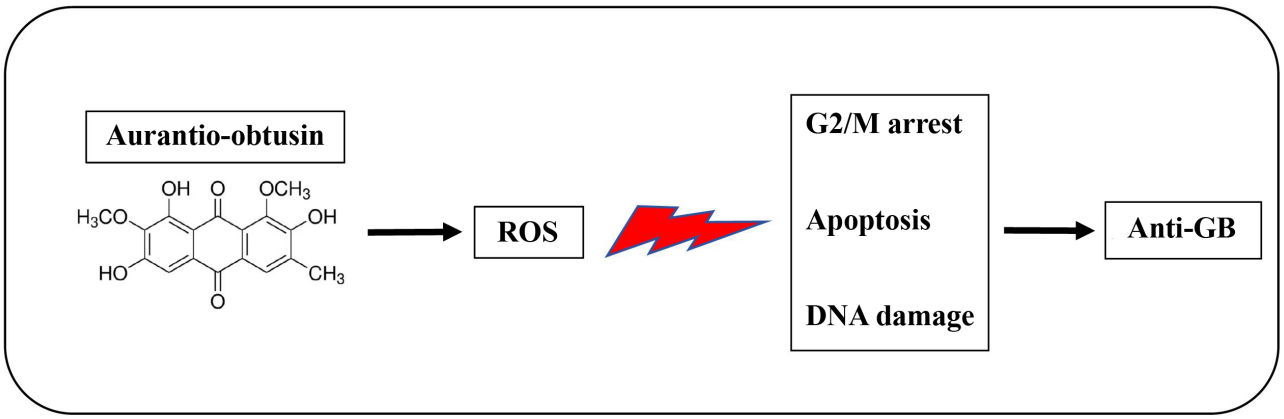


Fig. 6. AO inhibits the malignant progression of GB by inducing ROS generation.

marked increase in γ-H2AX. The dual consequences of the ROS burst are the arrest of the G2/M phase and the induction of mitochondrial apoptosis. Importantly, the antioxidant AC not only scavenged AO-induced ROS but also effectively reversed all downstream effects: Restored cell viability, alleviated G2/M phase arrest, suppressed apoptosis, and normalized the expression levels of p-cdc2, γ-H2AX, and cleaved caspase-3. This series of experiments provides compelling evidence that ROS generation is not merely an associated event but is the central mechanistic driver of AO's cytotoxicity in GB cells.

5. Study Limitations

While our study establishes that AO exerts its anti-GB effects through ROS induction, several avenues warrant further exploration. First, the specific molecular target of AO that initiates ROS generation remains unidentified. Investigating whether AO interferes with mitochondrial electron transport chain complexes or inhibits antioxidant enzymes could provide deeper mechanistic insight. Second, the blood-brain barrier (BBB) penetration capability of AO, a critical factor for treating intracranial GB, was not assessed in this subcutaneous model. Future studies employing orthotopic GB models are essential to evaluate its efficacy and pharmacokinetics within the brain parenchyma. Finally, exploring potential combinations of AO with standard therapies like temozolomide or radiotherapy could reveal synergistic effects, especially given that radiation itself relies partly on ROS generation.

6. Conclusions

The current work provides the first evidence that AO suppression of tumor progression may be promoting ROS generation, inducing DNA damage, G2/M phase arrest, and apoptosis in GB, suggesting that AO might be a promising drug for the treatment of GB.

Availability of Data and Materials

The data during the current study are available from the corresponding authors on reasonable request.

Author Contributions

JL and JRZ performed the research and wrote the manuscript. XZ, AQ, LL, and JHZ analysed the data. ZZ and HZ designed the research and revised the manuscript. All authors agreed on the article submission and revised the manuscript. All authors read and approved the final manuscript. All authors have participated sufficiently in the work and agreed to be accountable for all aspects of the work.

Ethics Approval and Consent to Participate

All animal experiments were conducted using principles approved by the Guidelines for the Care and Use of Laboratory Animals of Southwest Medical University. The protocol was approved by the Ethics Committee of Southwest Medical University (approval no: 20240927-001 to Zhengjun Zhou). This study was reported in accordance with the ARRIVE guidelines. The ARRIVE checklist is provided in the **Supplementary Material**.

Acknowledgment

We would like to express our gratitude to all those who helped us during the writing of this manuscript.

Funding

This study was supported by University Science and Technology Strategic Cooperation Project (2024SNXNYD03 to Zhengjun Zhou).

Conflicts of Interest

The authors declare no conflicts of interest.

Supplementary Material

Supplementary material associated with this article can be found, in the online version, at https://doi.org/10.31083/JIN50938.

References

[1] Pouyan A, Ghorbanlo M, Eslami M, Jahanshahi M, Ziaei E, Salami A, et al. Glioblastoma multiforme: insights into pathogenesis, key signaling pathways, and therapeutic strategies. Molecular Cancer. 2025; 24: 58. https://doi.org/10.1186/s12943-025-02267-0

[2] Horschitz S, Jabali A, Heuer S, Zillich E, Zillich L, Hoffmann DC, et al. Development of a fully human glioblastoma-in-brain-spheroid model for accelerated translational research. Journal of Advanced Research. 2026; 79: 363–377. https://doi.org/10.1016/j.jare.2025.03.055

[3] Politis A, Stavrinou L, Kalyvas A, Boviatsis E, Piperi C. Glioblastoma: Molecular features, emerging molecular targets and novel therapeutic strategies. Critical Reviews in Oncology/hematology. 2025; 212: 104764. https://doi.org/10.1016/j.critrevonc.2025.104764

[4] Salbini M, Formato A, Mongiardi MP, Levi A, Falchetti ML. Kinase-Targeted Therapies for Glioblastoma. International Journal of Molecular Sciences. 2025; 26: 3737. https://doi.org/10.3390/ijms26083737

[5] Wang N, Qing Q, Xue Y, Cai S, Zheng M, Zhang D, et al. Enhancing lipid nanoparticles-mediated RNA delivery to glioblastoma via targeted strategies. Journal of Controlled Release: Official Journal of the Controlled Release Society. 2026; 389: 114472. https://doi.org/10.1016/j.jconrel.2025.114472

[6] Hawly J, Murcar MG, Schcolnik-Cabrera A, Issa ME. Glioblastoma stem cell metabolism and immunity. Cancer Metastasis Reviews. 2024; 43: 1015–1035. https://doi.org/10.1007/s10555-024-10183-w

[7] Rana M, Liou KC, Thakur A, Nepali K, Liou JP. Advancing glioblastoma therapy: Learning from the past and innovations for the future. Cancer Letters. 2025; 617: 217601. https://doi.org/10.1016/j.canlet.2025.217601

[8] Xi Z, Dai R, Ze Y, Jiang X, Liu M, Xu H. Traditional Chinese medicine in lung cancer treatment. Molecular Cancer. 2025; 24: 57. https://doi.org/10.1186/s12943-025-02245-6

[9] Gaiaschi L, Bottone MG, De Luca F. Towards Effective Treatment of Glioblastoma: The Role of Combination Therapies and the Potential of Phytotherapy and Micotherapy. Current Issues in Molecular Biology. 2024; 46: 14324–14350. https://doi.org/10.3390/cimb46120859

[10] Gaiaschi L, De Luca F, Roda E, Ferrari B, Casali C, Inguscio CR, et al. A Phyto-mycotherapeutic Supplement, Namely *Ganostile*, as Effective Adjuvant in Brain Cancer Management: An In Vitro Study Using U251 Human Glioblastoma Cell Line. International Journal of Molecular Sciences. 2024; 25: 6204. https://doi.org/10.3390/ijms25116204

[11] Liu Y, Sun X, Hu X, Xu Y, Li T, Wu Z. Pharmacological properties and underlying mechanisms of aurantio-obtusin (Review). Experimental and Therapeutic Medicine. 2023; 26: 380. https://doi.org/10.3892/etm.2023.12079

[12] Hou J, Gu Y, Zhao S, Huo M, Wang S, Zhang Y, et al. Anti-Inflammatory Effects of Aurantio-Obtusin from Seed of *Cassia obtusifolia* L. through Modulation of the NF-κB Pathway. Molecules (Basel, Switzerland). 2018; 23: 3093. https://doi.org/10.3390/molecules23123093

[13] Li Z, Jin Y, Zhao H, Gu Y, Zhang Y, Cheng S, et al. Aurantio-Obtusin Regulates Gut Microbiota and Serum Metabolism to Alleviate High-Fat Diet-Induced Obesity-Associated Non-Alcoholic Fatty Liver Disease in Mice. Phytotherapy Research. 2025; 39: 1946–1965. https://doi.org/10.1002/ptr.8459

[14] Wu R, Liu R, Chen R, Li Y, Xue X, Zhang Y, et al. Aurantio-obtusin improves obesity and protects hepatic inflammation by rescuing mitochondrial damage in overwhelmed brown adipose tissue. Chinese Medicine. 2025; 20: 41. https://doi.org/10.1186/s13020-025-01097-y

[15] Li R, O'Connor DJ, Digby B, Broin PÓ, Hu X, Ge N, et al. Aurantio-obtusin modulates Wilms Tumour 1 within the breast tumour microenvironment reducing immunosuppression and tumour growth. Cell Communication and Signaling: CCS. 2025; 23: 309. https://doi.org/10.1186/s12964-025-02292-y

[16] Liu W, Deng J, Tao XJ, Peng Y, Chen XD, Qu XC, et al. Aurantio-obtusin regulates lipogenesis and ferroptosis of liver cancer cells through inhibiting SCD1 and sensitizing RSL3. International Journal of Oncology. 2024; 65: 92. https://doi.org/10.3892/ijo.2024.5680

[17] Zhang B, Pan C, Feng C, Yan C, Yu Y, Chen Z, et al. Role of mitochondrial reactive oxygen species in homeostasis regulation. Redox Report: Communications in Free Radical Research. 2022; 27: 45–52. https://doi.org/10.1080/13510002.2022.2046423

[18] Xie M, Fu X, Lan Y, Zhang Y, Li H, Su Y, et al. Spatially selective clearance of inflammation-mediated reactive oxygen species in injured kidney cells. Theranostics. 2026; 16: 1466–1481. https://doi.org/10.7150/thno.112905

[19] Sahoo BM, Banik BK, Borah P, Jain A. Reactive Oxygen Species (ROS): Key Components in Cancer Therapies. Anticancer Agents in Medicinal Chemistry. 2022; 22: 215–222. https://doi.org/10.2174/1871520621666210608095512

[20] Xing J, Lu W, Zhang Y, Yang C, Yang J, Shi J, et al. Design of prodrugs with reactive oxygen species as activators and their application in tumor therapy. Theranostics. 2026; 16: 1295–1327. https://doi.org/10.7150/thno.121977

[21] Chen CY, Ye YZ, Huang YH, Tzeng YM, Gurbanov R, Wang WL, et al. Ovatodiolide inhibits endometrial cancer stemness via reactive oxygen species-mediated DNA damage and cell cycle arrest. Chemico-biological Interactions. 2024; 403: 111244. https://doi.org/10.1016/j.cbi.2024.111244

[22] Tu Y, Zhou Y, Zhang D, Yang J, Li X, Ji K, et al. Light-Induced Reactive Oxygen Species (ROS) Generator for Tumor Therapy through an ROS Burst in Mitochondria and AKT-Inactivation-Induced Apoptosis. ACS Applied Bio Materials. 2021; 4: 5222–5230. https://doi.org/10.1021/acsabm.1c00386

[23] Chen Q, Zu M, Gong H, Ma Y, Sun J, Ran S, et al. Tea leaf-derived exosome-like nanotherapeutics retard breast tumor growth by pro-apoptosis and microbiota modulation. Journal of Nanobiotechnology. 2023; 21: 6. https://doi.org/10.1186/s12951-022-01755-5

[24] Liu Y, Liu X, Wang H, Ding P, Wang C. Agrimonolide inhibits cancer progression and induces ferroptosis and apoptosis by targeting SCD1 in ovarian cancer cells. Phytomedicine: International Journal of Phytotherapy and Phytopharmacology. 2022; 101: 154102. https://doi.org/10.1016/j.phymed.2022.154102

[25] Zhang X, Shao X, Bao Q, He L, Qi X. Integrated network pharmacology and experimental verification to reveal the role of Shezhi Huangling Decoction against glioma by inactivating PI3K/Akt-HIF1A axis. Heliyon. 2024; 10: e34215. https://doi.org/10.1016/j.heliyon.2024.e34215

[26] Tu X, Wang CC. The involvement of two cdc2-related kinases (CRKs) in Trypanosoma brucei cell cycle regulation and the distinctive stage-specific phenotypes caused by CRK3 depletion. The Journal of Biological Chemistry. 2004; 279: 20519–20528. https://doi.org/10.1074/jbc.M312862200

[27] Fletcher L, Cheng Y, Muschel RJ. Abolishment of the Tyr-15 inhibitory phosphorylation site on cdc2 reduces the radiation-induced G(2) delay, revealing a potential checkpoint in early

mitosis. Cancer Research. 2002; 62: 241–250.
[28] Zhang P, Huang CR, Wang W, Zhang XK, Chen JJ, Wang JJ, et al. Harmine Hydrochloride Triggers G2 Phase Arrest and Apoptosis in MGC-803 Cells and SMMC-7721 Cells by Upregulating p21, Activating Caspase-8/Bid, and Downregulating ERK/Bad Pathway. Phytotherapy Research: PTR. 2016; 30: 31–40. https://doi.org/10.1002/ptr.5497
[29] Gurung SK, Kumari S, Dana S, Mandal K, Sen S, Mukhopadhyay P, et al. DNA damage, cell cycle perturbation and cell death by naphthalene diimide derivative in gastric cancer cells. Chemico-biological Interactions. 2022; 358: 109881. https://doi.org/10.1016/j.cbi.2022.109881
[30] Kim TW. Nodakenin Induces ROS-Dependent Apoptotic Cell Death and ER Stress in Radioresistant Breast Cancer. Antioxidants (Basel, Switzerland). 2023; 12: 492. https://doi.org/10.3390/antiox12020492
[31] Xie X, Li Z, Tang H, Zhang Y, Huang Y, Zhang F, et al. A homologous membrane-camouflaged self-assembled nanodrug for synergistic antitumor therapy. Acta Biomaterialia. 2024; 183: 292–305. https://doi.org/10.1016/j.actbio.2024.05.049
[32] Roman A, Motoc A, Marcovici I, Dehelean C, Nicolescu L, Boru C. Genistein Improves the Cytotoxic, Apoptotic, and Oxidative-Stress-Inducing Properties of Doxorubicin in SK-MEL-28 Cancer Cells. Medicina (Kaunas, Lithuania). 2025; 61: 798. https://doi.org/10.3390/medicina61050798
[33] Zhou Y, Zeng L, Cai L, Zheng W, Liu X, Xiao Y, et al. Cellular senescence-associated gene IFI16 promotes HMOX1-dependent evasion of ferroptosis and radioresistance in glioblastoma. Nature Communications. 2025; 16: 1212. https://doi.org/10.1038/s41467-025-56456-y
[34] Lang F, Cornwell JA, Kaur K, Elmogazy O, Zhang W, Zhang M, et al. Abrogation of the G2/M checkpoint as a chemosensitization approach for alkylating agents. Neuro-oncology. 2024; 26: 1083–1096. https://doi.org/10.1093/neuonc/noad252
[35] Li S, Li Q, Lv X, Liao L, Yang W, Li S, et al. Aurantio-obtusin relaxes systemic arteries through endothelial PI3K/AKT/eNOS-dependent signaling pathway in rats. Journal of Pharmacological Sciences. 2015; 128: 108–115. https://doi.org/10.1016/j.jphs.2015.05.006
[36] Moosavi F, Firoozi R, Tavakkoli M, Nazari S, Alipour A, Firuzi O. Combination of chemotherapy and c-MET inhibitors has synergistic effects in c-MET overexpressing pancreatic cancer cells. Biochimie. 2025; 231: 73–83. https://doi.org/10.1016/j.biochi.2024.12.006